

# Quantitative PET Analysis of the Dopamine D<sub>2</sub> Receptor Agonist Radioligand <sup>11</sup>C-(R)-2-CH<sub>3</sub>O-N-n-Propylnorapomorphine in the Human Brain

Tatsui Otsuka<sup>1,2</sup>, Hiroshi Ito<sup>1</sup>, Christer Halldin<sup>3</sup>, Hidehiko Takahashi<sup>1</sup>, Harumasa Takano<sup>1</sup>, Ryosuke Arakawa<sup>1</sup>, Masaki Okumura<sup>1</sup>, Fumitoshi Kodaka<sup>1</sup>, Michie Miyoshi<sup>1</sup>, Mizuho Sekine<sup>1</sup>, Chie Seki<sup>1</sup>, Ryuji Nakao<sup>4</sup>, Kazutoshi Suzuki<sup>4</sup>, Sjoerd Finnema<sup>3</sup>, Yoshio Hirayasu<sup>2</sup>, Tetsuya Suhara<sup>1</sup>, and Lars Farde<sup>3</sup>

<sup>1</sup>Molecular Neuroimaging Group, Molecular Imaging Center, National Institute of Radiological Sciences, Chiba, Japan;

<sup>2</sup>Department of Psychiatry, Yokohama City University School of Medicine, Yokohama, Japan; <sup>3</sup>Psychiatry Section, Department of Clinical Neuroscience, Karolinska Institutet, Karolinska Hospital, Stockholm, Sweden; and <sup>4</sup>Molecular Probe Group, Molecular Imaging Center, National Institute of Radiological Sciences, Chiba, Japan

It has been demonstrated in vitro that the dopamine D<sub>2</sub> receptor has 2 interconvertible affinity states for endogenous dopamine, referred to as the high- and the low-affinity states. <sup>11</sup>C-(R)-2-CH<sub>3</sub>O-N-n-propylnorapomorphine (<sup>11</sup>C-MNPA) is a new agonist radioligand for in vivo imaging of the high-affinity state of dopamine D<sub>2</sub> receptors using PET. In the present study, the kinetics of <sup>11</sup>C-MNPA were examined for the first time, to our knowledge, in the human brain and analyzed using quantitative approaches with or without an arterial input function. **Methods:** A 90-min dynamic PET scan was obtained for 10 healthy men after an intravenous injection of <sup>11</sup>C-MNPA. The binding potential (BP<sub>ND</sub>) was calculated using the indirect kinetic method, a kinetic compartment analysis with a metabolite-corrected arterial input function. BP<sub>ND</sub> was also calculated by the simplified reference tissue model (SRTM) and transient equilibrium methods, both with the cerebellum as the reference brain region. The results of the quantitative methods were compared in a cross-validation approach. **Results:** The highest regional radioactivity was observed in the putamen. BP<sub>ND</sub> values obtained by kinetic analysis were  $0.82 \pm 0.09$ ,  $0.59 \pm 0.11$ , and  $0.28 \pm 0.06$ , respectively, in the putamen, caudate, and thalamus. BP<sub>ND</sub> values obtained by the SRTM and transient equilibrium methods were in good agreement with those obtained by the indirect kinetic method ( $r = 0.98$  and  $r = 0.93$ , respectively). For all quantification methods, the BP<sub>ND</sub> values based on data acquired from 0 to 60 min were in good agreement with those based on data acquired from 0 to 90 min ( $r = 0.90$ – $0.99$ ). **Conclusion:** The regional distribution of <sup>11</sup>C-MNPA binding was in good agreement with previous PET studies of dopamine D<sub>2</sub> receptors in the human brain using antagonist radioligands. The results support routine use of the SRTM and transient equilibrium methods, that is, methods that do not require an arterial input function and need a scan time of only about 60 min. <sup>11</sup>C-MNPA should thus be useful for clinical

research on the pathophysiology of neuropsychiatric disorders and estimation of dopamine D<sub>2</sub> receptor occupancy by dopaminergic drugs.

**Key Words:** <sup>11</sup>C-MNPA; agonist; dopamine D<sub>2</sub> receptor; positron emission tomography; human

**J Nucl Med 2009; 50:703–710**

DOI: 10.2967/jnumed.108.058503

**T**he dopaminergic system in the brain plays a significant role in the physiologic regulation of motor functions, cognition, emotion, and personality (1). Alterations of dopaminergic neurotransmission have been implicated in several pathologic conditions, such as schizophrenia (2), Parkinson disease (3), and addiction (4). Dopamine receptors are classified into 5 subtypes, D<sub>1</sub>, D<sub>2</sub>, D<sub>3</sub>, D<sub>4</sub>, and D<sub>5</sub> (5). The dopamine D<sub>2</sub> receptor is a main therapeutic target for currently used antipsychotic drugs and has long been suggested to be involved in the pathophysiology of schizophrenia (2,6–11).

Several observations in vitro indicate that the dopamine D<sub>2</sub> receptor exists in 2 interconvertible affinity states, distinguished by the affinity of endogenous dopamine and referred to as the high- and low-affinity states. It has further been suggested that the high-affinity state is the functionally active form of the receptor and is thus more relevant for clinical studies (12). Studies of dopamine D<sub>2</sub> receptors using PET have almost exclusively been performed with antagonist radioligands, such as <sup>11</sup>C-raclopride and <sup>11</sup>C-FLB457 (13–15). Antagonist radioligands do, however, bind with equal affinity to the 2 conformational states of the dopamine D<sub>2</sub> receptor. To examine the high-affinity state of the dopamine D<sub>2</sub> receptor in vitro and in vivo, agonist radioligands such as (–)-N-<sup>11</sup>C-propyl-norapomorphine

Received Sep. 25, 2008; revision accepted Jan. 21, 2009.

For correspondence or reprints contact: Hiroshi Ito, Molecular Neuroimaging Group, Molecular Imaging Center, National Institute of Radiological Sciences 4-9-1, Anagawa, Inage-ku, Chiba, 263-8555, Japan.

E-mail: hito@nirs.go.jp

COPYRIGHT © 2009 by the Society of Nuclear Medicine, Inc.

( $^{11}\text{C}$ -NPA) and  $^{11}\text{C}$ -(-)-4-propyl-3,4,4a,5,6,10b-hexahydro-2H-naphtho[1,2-b][1,4]oxazin-9-ol ( $^{11}\text{C}$ -PHNO) have recently been developed (16,17).

$^{11}\text{C}$ -(R)-2-CH<sub>3</sub>O-N-n-propylnorapomorphine ( $^{11}\text{C}$ -MNPA) is another new agonist PET radioligand with high affinity and selectivity for the dopamine D<sub>2</sub> receptor (inhibitory concentration of 50%, 1.02 nM; inhibition constant 0.17 nM, respectively) (18,19) and was recently characterized in non-human primates (20). PET measurements in cynomolgus monkeys showed high uptake in the striatum, with a striatum-to-cerebellum ratio of 2:2. The striatal uptake of  $^{11}\text{C}$ -MNPA could be inhibited by the injection of unlabeled raclopride, confirming that the striatal binding is reversible and specific for dopamine D<sub>2</sub> receptors. Subsequent applied studies using amphetamine-induced dopamine release showed that  $^{11}\text{C}$ -MNPA was more sensitive than  $^{11}\text{C}$ -raclopride, thus supporting the indication that  $^{11}\text{C}$ -MNPA is a promising radioligand for PET of the high-affinity state of the dopamine D<sub>2</sub> receptor in vivo (21). The aim of the present study was to examine the regional distribution and kinetics of  $^{11}\text{C}$ -MNPA in the human brain. Ten control subjects were included, and data were analyzed using kinetic compartment analyses with a metabolite-corrected input function and 2 quantitative methods with the cerebellum as a reference brain region.

## MATERIALS AND METHODS

### Subjects

Ten healthy men (age range, 22–35 y; mean  $\pm$  SD, 27.7  $\pm$  5.4y) participated in this study. On the basis of their medical history and MRI of the brain, all subjects were free of any somatic, neurologic, or psychiatric disorders, and they had no history of current or previous drug abuse. Written informed consent was obtained from all subjects after the study was completely described. The study was approved by the Ethics and Radiation Safety Committee of the National Institute of Radiological Sciences, Chiba, Japan.

### PET Procedure

$^{11}\text{C}$ -MNPA was synthesized as described in detail previously (20). In brief,  $^{11}\text{C}$ -MNPA was synthesized by the methylation of (R)-(-)-2,10,11-trihydroxy-N-n-propylnorapomorphine-acetonide with  $^{11}\text{C}$ -methyl triflate and subsequent cleavage of the acetonide protecting group with the addition of hydrochloric acid. An ECAT EXACT HR+ PET system (CTI-Siemens) was used for all measurements. A head-fixation device was used to minimize head movements during data acquisition. A transmission scan for attenuation correction was obtained using a  $^{68}\text{Ge}$ - $^{68}\text{Ga}$  source. Dynamic PET scans were obtained after a 1-min intravenous slow bolus injection of  $^{11}\text{C}$ -MNPA (204.3–232.1 MBq; mean  $\pm$  SD, 219.3  $\pm$  8.2 MBq). The specific radioactivity of  $^{11}\text{C}$ -MNPA was 197.5–335.0 GBq/ $\mu\text{mol}$  (261.1  $\pm$  43.3 GBq/ $\mu\text{mol}$ ) at the time of injection. Brain radioactivity was measured from 0 to 90 min (20 s  $\times$  9, 1 min  $\times$  5, 2 min  $\times$  4, 4 min  $\times$  11, and 5 min  $\times$  6).

MR images of the brain were acquired with a 1.5-T MRI scanner (Gyrosan NT; Philips). T1-weighted images were obtained at 1-mm slices acquired in 3 dimensions.

### Arterial Blood Sampling and Metabolite Analysis

To obtain the arterial input function, a series of arterial blood samples were taken manually from a catheter 32 times

(2.5 mL  $\times$  22 times for the measurement of radioactivity concentration in whole blood and plasma; 5.0 mL  $\times$  10 times for the determination of the percentage of unchanged  $^{11}\text{C}$ -MNPA in plasma) during the 90-min PET scan. Each blood sample was centrifuged to obtain plasma and blood cell fractions, and the concentrations of radioactivity in whole blood and plasma were measured.

The percentage of unchanged  $^{11}\text{C}$ -MNPA in plasma was determined by high-performance liquid chromatography (HPLC) in 10 of the blood samples. Acetonitrile was added to each plasma sample, and the samples were then centrifuged. The supernatant was subjected to radio-HPLC analysis (column, XBridge Prep C18; Waters) (mobile phase, 48:52 90% acetonitrile:50 mM ammonium acetate). The arterial plasma input function was defined as the radioactivity of plasma multiplied by the percentage of unchanged radioligand.

### Regions of Interest (ROIs)

All MR images were coregistered to the PET images using the statistical parametric mapping system (SPM2; Wellcome Trust Centre for Neuroimaging) (22). ROIs were drawn manually on summated PET images with reference to the coregistered MR images. ROIs were defined for the cerebellar cortex, putamen, caudate, and thalamus. Regional radioactivity was calculated for each frame, corrected for decay, and plotted versus time.

### Kinetic Compartment Analysis of $^{11}\text{C}$ -MNPA Binding

To describe the kinetics of  $^{11}\text{C}$ -MNPA in the brain, the 2-tissue-compartment model with 4 rate constants,  $K_1$ ,  $k_2$ ,  $k_3$ , and  $k_4$ , was used. The 3 compartments include  $C_P$ , the radioactivity concentration of unchanged radioligand in plasma (arterial input function);  $C_{ND}$ , the radioactivity concentration of nondisplaceable radioligand in the brain (including nonspecifically bound and free radioligand); and  $C_S$ , the radioactivity concentration of radioligand specifically bound to receptors. The rate constants  $K_1$  and  $k_2$  represent the influx and efflux rates for radioligand diffusion across the blood–brain barrier. The rate constants  $k_3$  and  $k_4$  represent radioligand transfer between the compartments for nondisplaceable and specifically bound radioligand.

### Calculation of the $^{11}\text{C}$ -MNPA Binding Potential

$^{11}\text{C}$ -MNPA binding was expressed by the indirect kinetic, SRTM, and transient equilibrium methods. In these methods,  $^{11}\text{C}$ -MNPA bindings were expressed as binding relative to nondisplaceable binding ( $\text{BP}_{ND}$ ) (23). The  $\text{BP}_{ND}$  of the radioligand is proportional to the product of the receptor density ( $B_{\text{max}}$ ) and reciprocal affinity ( $1/K_d$ ), and the ratio of  $B_{\text{max}}$  to  $K_d$  corresponds to the ratio of  $k_3$  to  $k_4$ , as expressed by the following equation:

$$\text{BP}_{ND} = f_{ND}(B_{\text{max}}/K_d) = k_3/k_4, \quad \text{Eq. 1}$$

where  $f_{ND}$  is the free fraction of radioligand in the nondisplaceable compartment. The cerebellum (cerebellar cortex) was used as a reference brain region because it is a structure with negligible D<sub>2</sub> dopamine receptor density (24). The software package PMOD (PMOD Technologies) was used for the indirect kinetic, SRTM, and transient equilibrium quantitative methods.

**Indirect Kinetic Method.** In the present cross-validation approach, the indirect kinetic method was used as the standard method (25).  $\text{BP}_{ND}$  was defined as the ratio of  $k_3$  to  $k_4$  as calculated using the 2-tissue-compartment model. Because the ratio of  $k_3$  to  $k_4$  is sensitive for noise in the PET data,  $\text{BP}_{ND}$  was

calculated using the indirect kinetic method. With the cerebellum as a reference region,  $BP_{ND}$  can be expressed as:

$$BP_{ND} = V_{T(\text{region})}/V_{T(\text{cerebellum})} - 1, \quad \text{Eq. 2}$$

where  $V_{T(\text{region})}$  is the total distribution volume ( $= (K_1/k_2)(k_3/k_4 + 1)$ ) in a target region, and  $V_{T(\text{cerebellum})}$  is the total distribution volume ( $= K_1/k_2$ ) in the cerebellum. The rate constants  $K_1$ ,  $k_2$ ,  $k_3$ , and  $k_4$  in the putamen, caudate, and thalamus were determined by nonlinear curve fitting in a least-squares sense to the regional time-activity curves as described in the literature (15).  $K_1$  and  $k_2$  values in the cerebellum were also determined by nonlinear curve fitting in a least-squares sense but by using the 1-tissue-compartment model, assuming that the cerebellum has negligible  $D_2$  dopamine receptor density (24). To improve the stability of the curve fitting in the nonlinear curve-fitting procedure, the ratio of  $K_1$  to  $k_2$  was fixed for each subject to the value obtained in the cerebellum by the kinetic analysis with the 1-tissue-compartment model (range of  $K_1/k_2$ , 5.0–7.9 mL/cm<sup>3</sup>; mean  $\pm$  SD,  $6.5 \pm 0.75$  mL/cm<sup>3</sup>). In this analysis, blood volume, which depends on the first-pass extraction fraction of the tracer, was estimated using the radioactivity of whole blood to diminish the influence of tracer remaining in the blood (26).

**SRTM Method.** The SRTM method, assuming that both target and reference regions have the same level of nondisplaceable binding, can be used to interpret time-activity curves in the target region as follows (27):

$$C_T(t) = R_1 C_R(t) + (k_2 - R_1 k_2 / (1 + BP_{ND})) C_R(t) * \exp(-k_2 t / (1 + BP_{ND})), \quad \text{Eq. 3}$$

where  $C_T(t)$  is the total radioactivity concentration in a brain region measured by PET,  $R_1$  is the ratio of  $K_1$  to  $K_1'$  ( $K_1$ , influx rate constant for the brain region;  $K_1'$ , influx rate constant for the reference region),  $C_R(t)$  is the radioactivity concentration in the reference region (cerebellum), and  $*$  denotes the convolution integral. The parameters  $R_1$ ,  $k_2$ , and  $BP_{ND}$  in this model were estimated by the nonlinear curve-fitting procedure.

**Transient Equilibrium Method.** Transient equilibrium theoretically occurs when the derivative for specific binding ( $dC_S(t)/dt$ ) is 0, that is, the peak point of specific binding,  $C_S(t)$  (15,28). It follows that  $C_S(t)/C_{ND}(t)$  is equal to  $k_3/k_4$  ( $= BP_{ND}$ ) at transient equilibrium.

### Simulation Study

A simulation study was performed to estimate errors of  $BP_{ND}$  calculated by the SRTM and transient equilibrium methods. The assumed values and intervals examined were acquired from the results of the kinetic approach. Regional tissue time-activity curves (0–90 min) were generated according to the 2-tissue-compartment model. We assumed that the value of  $K_1/k_2$  equaled 6.6 mL/cm<sup>3</sup> and that of  $k_4$  equaled 0.18 min<sup>-1</sup>. The tissue time-activity curves were generated with  $K_1$  values between 0.20 and 0.60 mL/cm<sup>3</sup>/min in 6 steps and with  $k_3$  values between 0.02 and 0.20 min<sup>-1</sup> in 10 steps. A tissue time-activity curve for the cerebellum was generated according to the 1-tissue-compartment model with 2 rate constants, using 0.44 mL/cm<sup>3</sup>/min for  $K_1$  and 0.067 min<sup>-1</sup> for  $k_2$ . The average arterial input function ( $n = 10$ ), corrected for labeled metabolites, was used to generate the tissue time-activity curves.  $BP_{ND}$  was then calculated by applying the SRTM and transient equilibrium methods to the generated tissue

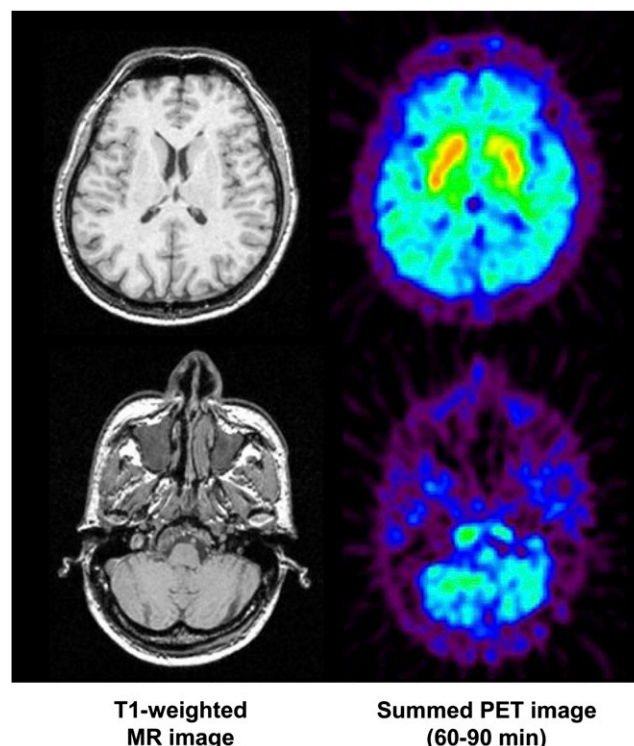


**FIGURE 1.** Representative summed PET images 60–90 min after intravenous injection of <sup>11</sup>C-MNPA (221 MBq) and corresponding T1-weighted MR images in control human subject. Upper panel shows horizontal section through striatum, and lower panel shows section through cerebellum.

time-activity curves. The estimated  $BP_{ND}$  values were compared with the  $BP_{ND}$  values calculated by the indirect kinetic method.

Variations in  $K_1$  values between a brain region and the cerebellum due to differences in cerebral blood flow (CBF) between

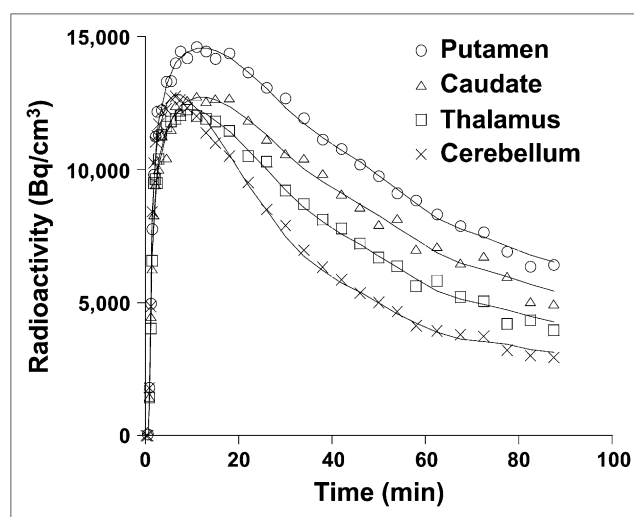


**FIGURE 2.** Representative regional time-activity curves after intravenous injection of <sup>11</sup>C-MNPA (232 MBq) binding in control human subject. Fitted curves using 2-tissue- and 1-tissue-compartment models are also shown for target regions and cerebellum, respectively.



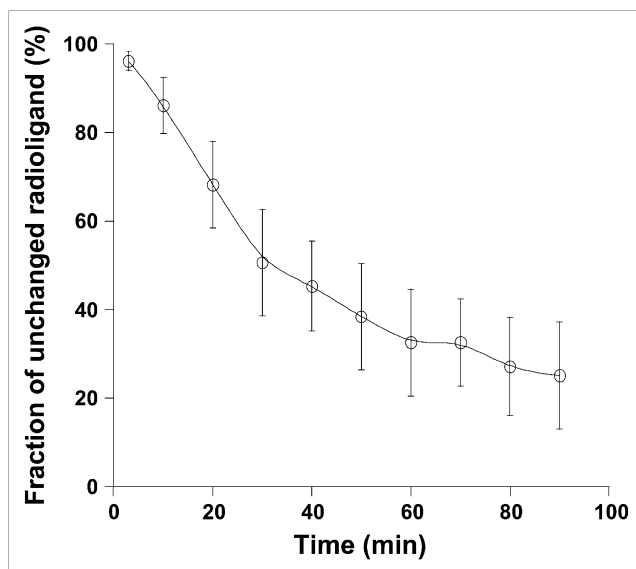


**FIGURE 3.** Average ( $n = 10$ ) percentage of unchanged  $^{11}\text{C}$ -MNPA in plasma vs. time. Bars indicate SD.

the 2 regions might affect the  $\text{BP}_{\text{ND}}$  calculated by the SRTM and transient equilibrium methods. Furthermore, changes in  $K_1$  due to changes in CBF might be caused by neurologic or psychiatric diseases. The  $K_1$  value for  $^{11}\text{C}$ -MNPA was about  $0.44 \text{ mL/cm}^3/\text{min}$  in gray matter. When the CBF value in gray matter is assumed to be  $0.50 \text{ mL/cm}^3/\text{min}$  (29), the first-pass extraction fraction of  $^{11}\text{C}$ -MNPA is 88%. The capillary permeability–surface area product (PS) value, using this extraction fraction and a  $K_1$  value of  $0.44 \text{ mL/cm}^3/\text{min}$ , was calculated (30,31). With the PS value of  $1.06 \text{ mL/cm}^3/\text{min}$ , the  $K_1$  range of  $0.20$ – $0.60 \text{ mL/cm}^3/\text{min}$  corresponds to the CBF range of  $0.20$ – $0.85 \text{ mL/cm}^3/\text{min}$  (28).

## RESULTS

All 10 subjects participated in the study according to the protocol. Representative summated PET images (60–90 min) and T1-weighted MR images are shown in Figure 1, and the corresponding regional time–activity curves are shown in Figure 2. Regional radioactivity was highest in the putamen and lower in the caudate and thalamus. The average percentage of unchanged  $^{11}\text{C}$ -MNPA in plasma was  $95.1\% \pm 2.1\%$  at 3 min, decreasing to  $25.1\% \pm 12.0\%$  at 90 min (i.e., at the end of PET data acquisition) (Fig. 3).

Other than MNPA, there were no more lipophilic-labeled metabolites in the plasma.

After an intravenous injection of  $^{11}\text{C}$ -MNPA, total radioactivity in the brain peaked at  $6.7 \pm 1.2$  min (range, 4.5–9.0 min), and the fraction of uptake in the brain was  $6.0\% \pm 1.0\%$  (range, 4.3%–7.3%) of the injected radioactivity.

The blood volume and rate constants for each brain region obtained by conventional nonlinear least-squares fit of the 2-compartment model are shown in Table 1. The  $\text{BP}_{\text{ND}}$  values of the putamen, caudate, and thalamus calculated by the 3 different methods are shown in Table 2. Specific binding, as defined by the transient equilibrium method, reached a peak within 60 min in the putamen, caudate, and thalamus (Table 2).

$\text{BP}_{\text{ND}}$  values determined by the SRTM method on the basis of data acquired for 90 and 60 min and those determined by the transient equilibrium method were compared with values calculated by the indirect kinetic method.  $\text{BP}_{\text{ND}}$  values obtained by the SRTM method were in good agreement with those obtained by the indirect kinetic method with data obtained for 90 and 60 min (Fig. 4), and  $\text{BP}_{\text{ND}}$  values obtained by the transient equilibrium method were in good agreement with those obtained by the indirect kinetic method with data for 90 min (Fig. 5). The highest coefficient of correlation was observed between the SRTM and the indirect kinetic methods with data acquired for 90 min ( $r = 0.98$ ,  $P < 0.001$ ).

When  $\text{BP}_{\text{ND}}$  values determined by the indirect kinetic and SRTM methods with 60-min data were compared with values determined by the same 2 methods with 90-min data, good agreement was observed ( $r = 0.99$ ,  $r = 0.92$ ,  $P < 0.001$ ) (Fig. 6).

To estimate the sensitivity of the SRTM and transient equilibrium methods for rate constants (indirect blood flow) over an interval with values lower and higher than average, a simulation study was performed.  $\text{BP}_{\text{ND}}$  values determined by the indirect kinetic method with data acquired for 60 and 90 min were compared with  $\text{BP}_{\text{ND}}$  values determined by the SRTM and transient equilibrium methods with data acquired for 60 and 90 min from simulated time–activity curves. The error in  $\text{BP}_{\text{ND}}$  calculated by the SRTM method with data acquired for 90 min was smallest ( $-24.8\%$  to  $1.5\%$ ; mean,  $-4.3\%$ ), and the difference in  $K_1$  between the brain region and cerebellum had only a minor effect on

**TABLE 1.** Rate Constants Obtained by Conventional Nonlinear Least-Squares Fit of 2-Tissue-Compartment Model

Region	Blood volume	Rate constant			
		$K_1$ ( $\text{mL/cm}^3/\text{min}$ )	$k_2$ ( $\text{min}^{-1}$ )	$k_3$ ( $\text{min}^{-1}$ )	$k_4$ ( $\text{min}^{-1}$ )
Putamen	$0.07 \pm 0.02$	$0.44 \pm 0.05$	$0.07 \pm 0.01$	$0.15 \pm 0.06$	$0.19 \pm 0.07$
Caudate	$0.06 \pm 0.02$	$0.39 \pm 0.05$	$0.06 \pm 0.01$	$0.11 \pm 0.06$	$0.20 \pm 0.11$
Thalamus	$0.07 \pm 0.02$	$0.43 \pm 0.05$	$0.07 \pm 0.01$	$0.03 \pm 0.01$	$0.13 \pm 0.06$
Cerebellum (1TCM)	$0.07 \pm 0.02$	$0.41 \pm 0.03$	$0.06 \pm 0.01$		

1TCM = 1-tissue-compartment model.  
Values are mean  $\pm$  SD.

**TABLE 2.** BP<sub>ND</sub> Values Obtained by Different Methods and Scan Times

Region	Indirect kinetic method		SRTM method		Transient equilibrium method	
	90 min	60 min	90 min	60 min	BP <sub>ND</sub>	Time (min)*
Putamen	0.82 ± 0.09	0.83 ± 0.09	0.78 ± 0.07	0.79 ± 0.08	0.76 ± 0.07	36.4 ± 4.5
Caudate	0.59 ± 0.11	0.59 ± 0.10	0.55 ± 0.09	0.56 ± 0.13	0.60 ± 0.09	39.6 ± 5.7
Thalamus	0.28 ± 0.06	0.28 ± 0.05	0.24 ± 0.04	0.31 ± 0.18	0.23 ± 0.05	29.2 ± 11.3

\*Time of transient equilibrium (min).  
Values are mean ± SD.

BP<sub>ND</sub>. The error in BP<sub>ND</sub> calculated by the transient equilibrium method was smallest when the  $K_1$  value was 0.44, but BP<sub>ND</sub> was overestimated when the  $K_1$  value was lower than 0.36 and was underestimated when it was higher than 0.52 (Fig. 7).

## DISCUSSION

Studies using agonist radioligands such as <sup>11</sup>C-PHNO to examine the high-affinity state of the dopamine D<sub>2</sub> receptor in the human brain have been reported previously (32). Our study describes the first, to our knowledge, PET examination using the agonist radioligand <sup>11</sup>C-MNPA to visualize binding to G-protein-coupled receptors in the human brain. After the intravenous injection of <sup>11</sup>C-MNPA, radioactivity appeared rapidly in the brain and was washed out in a fashion similar to that previously reported in nonhuman primates (20). Radioactivity was highest in the putamen and slightly lower in the caudate, moderate in the thalamus, and lowest in the cerebellum. This regional distribution is similar to that shown in nonhuman primates with <sup>11</sup>C-MNPA (20,21) and is in accordance with the known distribution of dopamine D<sub>2</sub> receptors, as demonstrated with antagonist radioligands such as <sup>11</sup>C-raclopride in the human brain (33). Finnema also reported blocking data with a dopamine D<sub>2</sub> antagonist in nonhuman primates (20). The pretreatment with raclopride, compared with the baseline condition, demonstrated high specific binding of the

dopamine D<sub>2</sub> receptor by reducing the striatum-to-cerebellum ratio. The striatal BP<sub>ND</sub> values of <sup>11</sup>C-MNPA were about one third of those in previous studies with the antagonist radioligand <sup>11</sup>C-raclopride (33). The  $K_d$  value of <sup>11</sup>C-raclopride in the human brain in vivo has been reported to be 9.1 nM (34), and the  $K_d$  value of <sup>11</sup>C-MNPA in the monkey brain in vivo has been reported to be 11.6 nM (35). Because the  $K_d$  values of <sup>11</sup>C-MNPA and <sup>11</sup>C-raclopride are similar in vitro, the difference in striatal BP<sub>ND</sub> between <sup>11</sup>C-MNPA and <sup>11</sup>C-raclopride may reflect a difference in the density of available receptors ( $B_{max}$ ) of the 2 radioligands. This interpretation is in line with the view that an agonist radioligand labels only the receptors in the high-affinity state, whereas an antagonist radioligand labels both high- and low-affinity-state dopamine D<sub>2</sub> receptors (21,35).

Genovart et al. reported that <sup>11</sup>C-PHNO and <sup>11</sup>C-NPA in the cat were more sensitive to amphetamine-induced dopamine release than was <sup>11</sup>C-raclopride (36). The observation that <sup>11</sup>C-MNPA in nonhuman primates is also more sensitive to amphetamine-induced dopamine release than is <sup>11</sup>C-raclopride (21) has been taken as evidence for selective labeling of D<sub>2</sub> receptors in the high-affinity state. The relatively low BP<sub>ND</sub> in the present study corroborates this view.

In this study, the indirect kinetic method with arterial blood sampling was used as the gold standard (25). Because arterial blood sampling is invasive, we examined the accuracy of the SRTM and transient equilibrium methods

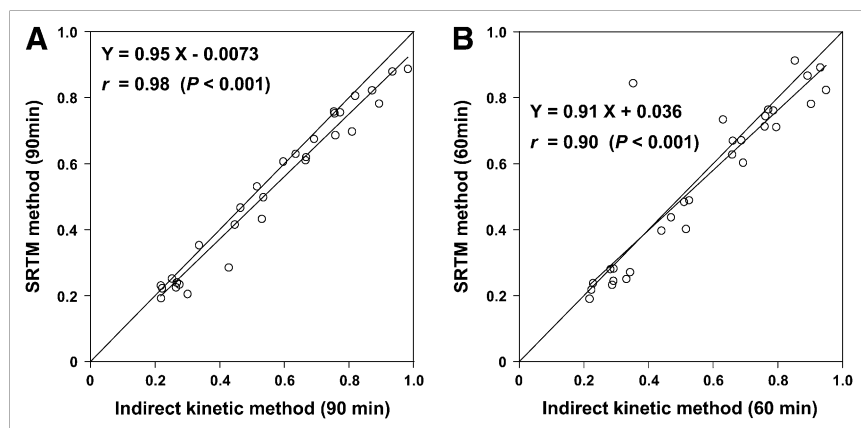


**FIGURE 4.** Comparison of BP<sub>ND</sub> values in 3 regions (putamen, caudate, and thalamus) of 10 control subjects calculated by indirect kinetic and SRTM methods on the basis of data acquired over 90 (A) and 60 min (B).

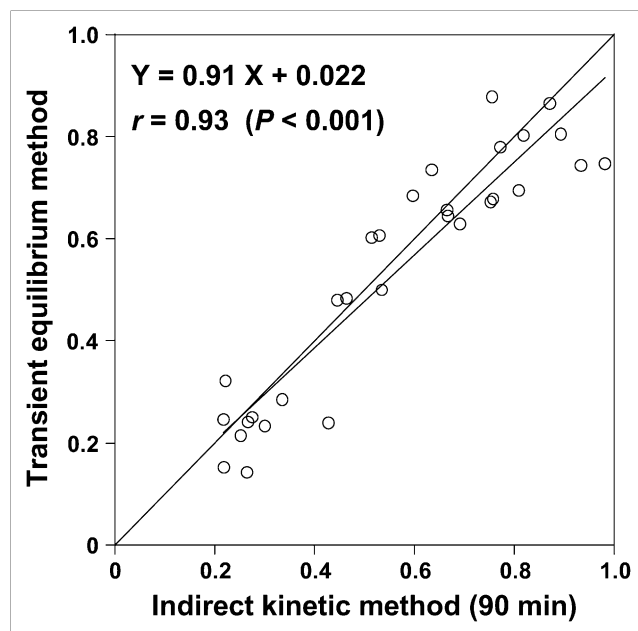


**FIGURE 5.** Comparison of  $BP_{ND}$  values in 3 regions (putamen, caudate, and thalamus) in 10 control subjects calculated by indirect kinetic and transient equilibrium methods.

for quantifying  $^{11}\text{C}$ -MNPA binding using the cerebellum as the reference brain region. The SRTM and transient equilibrium methods had previously been validated for antagonist radioligands such as  $^{11}\text{C}$ -raclopride and  $^{11}\text{C}$ -FLB457 (15,25,28). In the present study,  $BP_{ND}$  of  $^{11}\text{C}$ -MNPA obtained by the SRTM method was in good agreement with that obtained by the indirect kinetic method with data acquired for 60 and 90 min. The  $BP_{ND}$  value obtained by the transient equilibrium method was also in good agreement with the value obtained by the indirect kinetic method with data acquired for 90 min. Thus, it should be possible to use simplified protocols with no arterial blood sampling in applied clinical studies in humans.

In the simulation study,  $BP_{ND}$  calculated by the SRTM method was in good agreement with that calculated by the

indirect kinetic method, although  $BP_{ND}$  was slightly overestimated. These results demonstrate the validity of the SRTM method for quantitating  $^{11}\text{C}$ -MNPA binding also when blood flow and rate constants might be deviant. The present observation is in line with an  $^{11}\text{C}$ -FLB457 study showing that the  $BP_{ND}$  value calculated by the SRTM method was not greatly affected by differences in  $K_1$  between the brain regions and the cerebellum (25). Thus, the SRTM method is suitable for quantifying  $^{11}\text{C}$ -MNPA binding when using a reference brain region without arterial blood sampling.

$BP_{ND}$  calculated by the transient equilibrium method was not in good agreement with that calculated by the indirect kinetic method in the simulation study when the  $K_1$  value in the brain region was small. The errors in  $BP_{ND}$  calculated by the transient equilibrium method were within the range of  $-15\%$  to  $+15\%$  when the  $K_1$  value was 0.44 and 0.52  $\text{mL}/\text{cm}^3/\text{min}$ , corresponding to 0.5–0.65  $\text{mL}/\text{cm}^3/\text{min}$  of CBF. Although the transient equilibrium method might not be suitable for determining  $BP_{ND}$  in patients with low CBF, it is still a useful method for determining  $BP_{ND}$  without arterial blood sampling.

For clinical research, a short scanning time is preferred. In the present study, the  $BP_{ND}$  values calculated by the SRTM method with data acquired for 90 min were in good agreement with those obtained with data acquired for 60 min. In the simulation study, the  $BP_{ND}$  values obtained by the SRTM method with data acquired for 60 min were in good agreement with  $BP_{ND}$  values obtained by the indirect kinetic method, except with extremely low  $K_1$ . These results suggest that the SRTM method with data acquired for 60 min is valid for clinical studies in patients with neuropsychiatric disorders such as schizophrenia and depression.

## CONCLUSION

The regional distribution of  $^{11}\text{C}$ -MNPA was in good agreement with previous PET studies of dopamine  $D_2$  receptors in the human brain using antagonist radioligands such as  $^{11}\text{C}$ -raclopride and  $^{11}\text{C}$ -FLB457. The  $BP_{ND}$  values

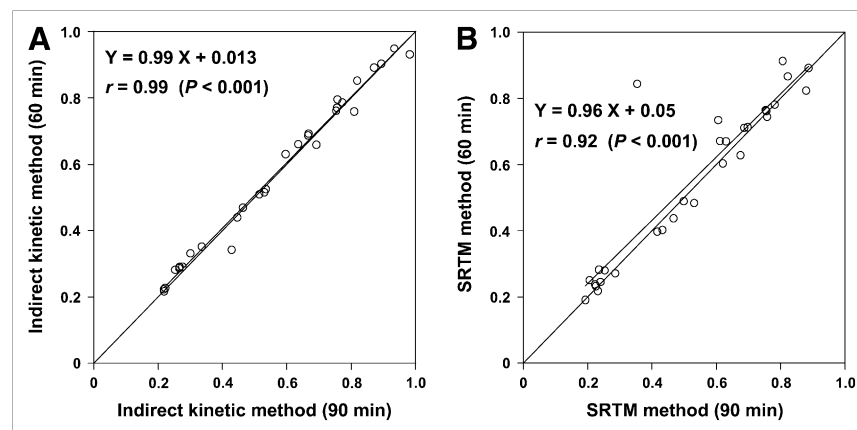


**FIGURE 6.** Comparison of  $BP_{ND}$  values in 3 regions (putamen, caudate, and thalamus) in 10 control subjects calculated by indirect kinetic (A) and SRTM (B) methods on the basis of data acquired over 90 and 60 min.

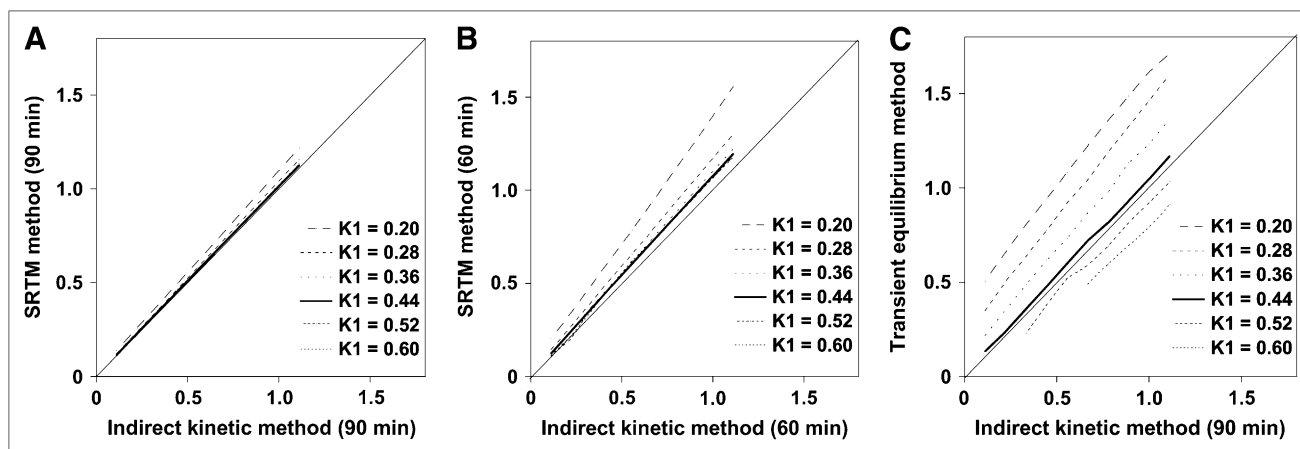


**FIGURE 7.** Comparison of simulated  $BP_{ND}$  values calculated by indirect kinetic and SRTM methods on the basis of data acquired over 90 (A) and 60 min (B). (C) Comparison of simulated  $BP_{ND}$  values calculated by indirect kinetic and transient equilibrium methods.

measured by the indirect kinetic model were in good agreement with those measured by the SRTM method with data acquired for 60 and 90 min. The  $BP_{ND}$  values measured by the transient equilibrium method also corresponded well with those measured by the indirect kinetic model with data acquired for 90 min. Simulation studies showed that errors in  $BP_{ND}$  measured by the SRTM method were small. The SRTM method with data acquired for 60 and 90 min is suitable for estimation of dopamine  $D_2$  receptor bindings using  $^{11}C$ -MNPA.

## ACKNOWLEDGMENTS

We thank Katsuyuki Tanimoto, Takahiro Shiraishi, and Akira Ando for their assistance in performing the PET experiments at the National Institute of Radiological Sciences. We also thank Yoshiko Fukushima of the National Institute of Radiological Sciences for her help as clinical research coordinator. This study was supported by a consignment expense for the Molecular Imaging Program on "Research Base for PET Diagnosis" from the Ministry of Education, Culture, Sports, Science and Technology, Japanese government.

## REFERENCES

- Montague PR, Hyman SE, Cohen JD. Computational roles for dopamine in behavioural control. *Nature*. 2004;431:760–767.
- Carlsson A. Antipsychotic drugs, neurotransmitters, and schizophrenia. *Am J Psychiatry*. 1978;135:165–173.
- Ehringer H, Hornykiewicz O. *Klin Wochenschr*. 1960;38:1236–1239.
- Volkow ND, Fowler JS, Wang GJ, Swanson JM. Dopamine in drug abuse and addiction: results from imaging studies and treatment implications. *Mol Psychiatry*. 2004;9:557–569.
- Strange PG. New insights into dopamine receptors in the central nervous system. *Neurochem Int*. 1993;22:223–236.
- Takano A, Suhara T, Ikoma Y, et al. Estimation of the time-course of dopamine  $D_2$  receptor occupancy in living human brain from plasma pharmacokinetics of antipsychotics. *Int J Neuropsychopharmacol*. 2004;7:19–26.
- Yasuno F, Suhara T, Okubo Y, et al. Low dopamine  $D_2$  receptor binding in subregions of the thalamus in schizophrenia. *Am J Psychiatry*. 2004;161:1016–1022.
- Suhara T, Okubo Y, Yasuno F, et al. Decreased dopamine  $D_2$  receptor binding in the anterior cingulate cortex in schizophrenia. *Arch Gen Psychiatry*. 2002;59:25–30.
- Yasuno F, Suhara T, Okubo Y, et al. Dose relationship of limbic-cortical  $D_2$ -dopamine receptor occupancy with risperidone. *Psychopharmacology (Berl)*. 2001;154:112–114.
- Talvik M, Nordstrom AL, Okubo Y, et al. Dopamine  $D_2$  receptor binding in drug-naïve patients with schizophrenia examined with [ $^{11}C$ ]raclopride and positron emission tomography. *Psychiatry Res*. 2006;148:165–173.
- Talvik M, Nordstrom AL, Olsson H, Halldin C, Farde L. Decreased thalamic  $D_2/D_3$  receptor binding in drug-naïve patients with schizophrenia: a PET study with [ $^{11}C$ ]FLB 457. *Int J Neuropsychopharmacol*. 2003;6:361–370.
- Sibley DR, De Lean A, Creese I. Anterior pituitary dopamine receptors: demonstration of interconvertible high and low affinity states of the  $D_2$  dopamine receptor. *J Biol Chem*. 1982;257:6351–6361.
- Halldin C, Gulyas B, Langer O, Farde L. Brain radioligands: state of the art and new trends. *Q J Nucl Med*. 2001;45:139–152.
- Olsson H, Halldin C, Swahn CG, Farde L. Quantification of [ $^{11}C$ ]FLB 457 binding to extrastriatal dopamine receptors in the human brain. *J Cereb Blood Flow Metab*. 1999;19:1164–1173.
- Farde L, Eriksson L, Blomquist G, Halldin C. Kinetic analysis of central [ $^{11}C$ ]raclopride binding to  $D_2$ -dopamine receptors studied by PET: a comparison to the equilibrium analysis. *J Cereb Blood Flow Metab*. 1989;9:696–708.
- Hwang DR, Kegeles LS, Laruelle M. (-)-N-[ $^{11}C$ ]propyl-norapomorphine: a positron-labeled dopamine agonist for PET imaging of  $D_2$  receptors. *Nucl Med Biol*. 2000;27:533–539.
- Wilson AA, McCormick P, Kapur S, et al. Radiosynthesis and evaluation of [ $^{11}C$ ]-(+)-4-propyl-3,4,4a,5,6,10b-hexahydro-2H-naphtho[1,2-b][1,4]oxazin-9-ol as a potential radiotracer for in vivo imaging of the dopamine  $D_2$  high-affinity state with positron emission tomography. *J Med Chem*. 2005;48:4153–4160.
- Gao YG, Baldessarini RJ, Kula NS, Neumeyer JL. Synthesis and dopamine receptor affinities of enantiomers of 2-substituted apomorphines and their N-n-propyl analogues. *J Med Chem*. 1990;33:1800–1805.
- Neumeyer JL, Gao YG, Kula NS, Baldessarini RJ. Synthesis and dopamine receptor affinity of (R)-(-)-2-fluoro-N-n-propylnorapomorphine: a highly potent and selective dopamine  $D_2$  agonist. *J Med Chem*. 1990;33:3122–3124.
- Finnema SJ, Seneca N, Farde L, et al. A preliminary PET evaluation of the new dopamine  $D_2$  receptor agonist [ $^{11}C$ ]MNPA in cynomolgus monkey. *Nucl Med Biol*. 2005;32:353–360.
- Seneca N, Finnema SJ, Farde L, et al. Effect of amphetamine on dopamine  $D_2$  receptor binding in nonhuman primate brain: a comparison of the agonist radioligand [ $^{11}C$ ]MNPA and antagonist [ $^{11}C$ ]raclopride. *Synapse*. 2006;59:260–269.

22. Friston KJ, Frith CD, Liddle PF, Dolan RJ, Lammertsma AA, Frackowiak RS. The relationship between global and local changes in PET scans. *J Cereb Blood Flow Metab.* 1990;10:458–466.
23. Innis RB, Cunningham VJ, Delforge J, et al. Consensus nomenclature for in vivo imaging of reversibly binding radioligands. *J Cereb Blood Flow Metab.* 2007;27:1533–1539.
24. Martres MP, Bouthenet ML, Sales N, Sokoloff P, Schwartz JC. Widespread distribution of brain dopamine receptors evidenced with [<sup>125</sup>I]iodosulpride, a highly selective ligand. *Science.* 1985;228:752–755.
25. Ito H, Sudo Y, Suhara T, Okubo Y, Halldin C, Farde L. Error analysis for quantification of [<sup>11</sup>C]FLB 457 binding to extrastriatal D<sub>2</sub> dopamine receptors in the human brain. *Neuroimage.* 2001;13:531–539.
26. Ito H, Ota M, Ikoma Y, et al. Quantitative analysis of dopamine synthesis in human brain using positron emission tomography with L-[beta-<sup>11</sup>C]DOPA. *Nucl Med Commun.* 2006;27:723–731.
27. Lammertsma AA, Hume SP. Simplified reference tissue model for PET receptor studies. *Neuroimage.* 1996;4:153–158.
28. Ito H, Hietala J, Blomqvist G, Halldin C, Farde L. Comparison of the transient equilibrium and continuous infusion method for quantitative PET analysis of [<sup>11</sup>C]raclopride binding. *J Cereb Blood Flow Metab.* 1998;18:941–950.
29. Hatazawa J, Fujita H, Kanno I, et al. Regional cerebral blood flow, blood volume, oxygen extraction fraction, and oxygen utilization rate in normal volunteers measured by the autoradiographic technique and the single breath inhalation method. *Ann Nucl Med.* 1995;9:15–21.
30. Renkin EM. Transport of potassium-42 from blood to tissue in isolated mammalian skeletal muscles. *Am J Physiol.* 1959;197:1205–1210.
31. Crone C. The permeability of capillaries in various organs as determined by use of the 'indicator diffusion' method. *Acta Physiol Scand.* 1963;58:292–305.
32. Willeit M, Ginovart N, Kapur S, et al. High-affinity states of human brain dopamine D<sub>2/3</sub> receptors imaged by the agonist [<sup>11</sup>C]-(+)-PHNO. *Biol Psychiatry.* 2006;59:389–394.
33. Ito H, Takahashi H, Arakawa R, Takano H, Suhara T. Normal database of dopaminergic neurotransmission system in human brain measured by positron emission tomography. *Neuroimage.* 2008;39:555–565.
34. Farde L, Hall H, Pauli S, Halldin C. Variability in D<sub>2</sub>-dopamine receptor density and affinity: a PET study with [<sup>11</sup>C]raclopride in man. *Synapse.* 1995;20:200–208.
35. Finnema SJ, Seneca N, Farde L, et al. Scatchard analysis of the D<sub>2</sub> receptor agonist [<sup>11</sup>C]MNPA in the monkey brain using PET [abstract]. *Eur J Nucl Med Mol Imaging.* 2005;32(S82):293.
36. Ginovart N, Galineau L, Willeit M, et al. Binding characteristics and sensitivity to endogenous dopamine of [<sup>11</sup>C]-(+)-PHNO, a new agonist radiotracer for imaging the high-affinity state of D<sub>2</sub> receptors in vivo using positron emission tomography. *J Neurochem.* 2006;97:1089–1103.





The Journal of  
NUCLEAR MEDICINE

## Quantitative PET Analysis of the Dopamine D<sub>2</sub> Receptor Agonist Radioligand <sup>11</sup>C-(R)-2-CH<sub>3</sub>O-N-n-Propylnorapomorphine in the Human Brain

Tatsui Otsuka, Hiroshi Ito, Christer Halldin, Hidehiko Takahashi, Harumasa Takano, Ryosuke Arakawa, Masaki Okumura, Fumitoshi Kodaka, Michie Miyoshi, Mizuho Sekine, Chie Seki, Ryuji Nakao, Kazutoshi Suzuki, Sjoerd Finnema, Yoshio Hirayasu, Tetsuya Suhara and Lars Farde

*J Nucl Med.* 2009;50:703-710.

Published online: April 16, 2009.

Doi: 10.2967/jnumed.108.058503

---

This article and updated information are available at:

<http://jnm.snmjournals.org/content/50/5/703>

---

Information about reproducing figures, tables, or other portions of this article can be found online at:

<http://jnm.snmjournals.org/site/misc/permission.xhtml>

Information about subscriptions to JNM can be found at:

<http://jnm.snmjournals.org/site/subscriptions/online.xhtml>

*The Journal of Nuclear Medicine* is published monthly.  
SNMMI | Society of Nuclear Medicine and Molecular Imaging  
1850 Samuel Morse Drive, Reston, VA 20190.  
(Print ISSN: 0161-5505, Online ISSN: 2159-662X)

© Copyright 2009 SNMMI; all rights reserved.

The logo for the Society of Nuclear Medicine and Molecular Imaging (SNMMI) consists of the letters 'S', 'N', 'M', and 'I' arranged in a 2x2 grid. Each letter is white and set within a red square.  
SOCIETY OF  
NUCLEAR MEDICINE  
AND MOLECULAR IMAGING